Improved Morphed Potentials for Ar−HBr Including Scaling to the Experimentally Determined Dissociation Energy

Z. Wang,[†] A. L. McIntosh,[†] B. A. McElmurry,[†] J. R. Walton,[‡] R. R. Lucchese,[†] and J. W. Bevan[†]

Chemistry and Mathematics Departments, Texas A&M University, College Station, Texas 77843-3255

Received: April 22, 2005; In Final Form: June 4, 2005

A lead salt diode infrared laser spectrometer has been employed to investigate the rotational predissociation in Ar−HBr for transitions up to $J' = 79$ in the υ_1 HBr stretching vibration of the complex using a slit jet and static gas phase. Line-shape analysis and modeling of the predissociation lifetimes have been used to determine a ground-state dissociation energy D_0 of 130(1) cm^{-1}. In addition, potential energy surfaces based on ab initio calculations are scaled, shifted, and dilated to generate three-dimensional morphed potentials for Ar−HBr that reproduce the measured value of D_0 and that have predictive capabilities for spectroscopic data with nearly experimental uncertainty. Such calculations also provide a basis for making a comprehensive comparison of the different morphed potentials generated using the methodologies applied.

I. Introduction

Recently, a number of studies[1−17] have considered the potential energy surfaces (PESs) in the sequence of molecules Ar−HX for X = F, Cl, Br, I. These studies have focused on this prototypical series that has been used to enhance understanding of the basic intermolecular forces that are important in a wide variety of processes in larger related rare gas clusters including photoinduced dissociation and cage effects.[18,19] The nature of the interaction changes substantially in this series as the properties of the X atom change in the HX components. In the complexes of the series under consideration, there is the possibility of two local minima in the interaction PES. One minimum in the PES occurs when the H atom is between the Ar and X, and this minimum will be referred to as the hydrogen bound (HB) isomer, Rg−HX. The other minimum in the PES has the H atom pointed away from the Ar atom and is referred to as the van der Waals (vdW) isomer, Rg−XH. Differences between the ground-state energies in these two forms, $\Delta E_0 = E_{0,vdW} - E_{0,HB}$, have been precisely determined and decrease down the series with increasing atomic number of X, becoming negative for X = I. Spectroscopically measured values or estimated values are 52.0565 cm^{-1} in Ar−HF, 23.6572 cm^{-1} in Ar−HCl,[9] 10.99465379(3) cm^{-1} in[11] Ar−H^{79}Br, and −8.777007483(33) cm^{-1} in[17] Ar−HI, respectively. As one proceeds down the periodic table, the vdW form thus becomes more stable with respect to the HB form. In Ar−HI, the vdW form is the most stable ground-state isomer, with the HB state of the dimer having been experimentally characterized using high-resolution submillimeter spectroscopy and demonstrated to be above the ground state of the complex.[17] Ar−HBr has been demonstrated to be of particular interest in this homologous series, as the ground rovibrational state of the potential was found to have the hydrogen-bound structure Ar−HBr. This state is 10.99465379(3) cm^{-1} more stable than the corresponding state having the vdW structure,[20] Ar−BrH. However, the global minimum of the morphed potential was shown to have the vdW structure, Ar−BrH, following the generation of an accurate fully 3D morphed PES for Ar−HBr based on an extensive range of spectroscopic data.[12] The vdW structure was initially predicted to be 20.9 cm^{-1} lower in energy than the local minimum having the HB structure. This dimer is thus an example of a molecular species at variance with the oft-held tenet in molecular structure, that atoms in the ground state and equilibrium structure of molecular species have the same structural arrangement as in this case and they correspond to different isomeric structures. More recently, investigations of Ar−HBr have been extended and predictive capabilities of the initially generated morphed potential tested by comparison with a very accurate analysis of the Σ bending transitions directly recorded using a coaxially configured submillimeter supersonic jet spectrometer.[11] The previously described value of 20.9 cm^{-1} was then refined to 23.7(30) cm^{-1} when this additional data was included in the fit. Morphed potentials were obtained from parametrized scaling and shifting transformations of an ab initio potential,[16,21] and optimum parameters of the morphed potential were determined by a regularized nonlinear least-squares fit to available experimental data.[12] The rovibrational dynamics of the complex were then computed using an adiabatic separation of the H−Br intramolecular stretching mode from the intermolecular modes of the system.[12]

Up to the present time, however, an accurate, experimentally based value for the ground-state dissociation energy of the Ar−HBr complex, D_0, has not been available for scaling purposes and inclusion in the optimization of morphed potentials. High-resolution spectroscopic or time-of-flight methods in molecular beams or supersonic jets have been employed to determine the vibrationally excited-state lifetimes of a number of Ar−HX complexes. These studies found relatively long-lived states in the case of low-lying rotational levels.[22−25] Consequently, the number of precisely determined dissociation energies evaluated using high-resolution spectroscopic methods in the near-infrared

* To whom correspondence should be addressed. E-mail: lucchese@mail.chem.tamu.edu.
[†] Chemistry Department, Texas A&M University.
[‡] Mathematics Department, Texas A&M University.

10.1021/jp0521104 CCC: $30.25
Published on Web 08/19/2005

have been limited[26] for this type of simple cluster though millimeter studies have been successfully used.[27] One viable approach to the determination of D_0 for Ar−HBr is using static gas-phase rotational predissociation investigations, similar to the successful studies of Ar−HF, Kr−HF, and Xe−HF.[28] Furthermore, recent discussion in the literature has focused on the advantages and disadvantages of the initially selected level of ab initio calculation for use in facilitating the generation of the preferable morphed potentials with the most accurate predictive capabilities.[15] In our initial studies of Ar−HBr, the *ab initio* calculations were performed at the second-order Møller−Plesset perturbation (MP2) level.[16] We will judge the efficacy of this approach by comparing morphed potentials based on MP2 and the more computationally demanding single and double excitation coupled cluster theory with perturbative treatment of triple excitations (CCSD(T)). Determination of an accurate ground-state dissociation energy for Ar−HBr would thus provide an important experimental parameter for characterizing this dimer. It also gives the opportunity for comparing directly the predictions of different levels of ab initio theory with additional experimental information[11,20] in a relatively simple system, for which there is an extensive spectroscopic database.

In this work, we report an extensive reanalysis of the rovibrational spectrum of the previously recorded[20] ν_1 vibration in Ar−H^{79}Br and Ar−H^{81}Br using a high-frequency wavelength modulation diode laser supersonic jet spectrometer. The spectrometer is used to extend the investigation of the spectrum and a detailed analysis of the variation of rotationally resolved line profiles of these rovibrational transitions in the static gas-phase spectrum up to $J' = 79$ for both isotopomers. A detailed investigation of rotational predissociation in these spectra provides the experimental basis for deriving an accurate determination of the ground-state dissociation energy of the complex based on the solution of the radial scattering equation. Predictions based on MP2 and CCSD(T) calculations will be compared with this and other spectroscopic data. Furthermore, the available experimental data will be used to make a critical evaluation of morphed potentials generated from these different *ab initio* potentials.

II. Experimental Section

The high-frequency wavelength modulation spectrometer used in the reported experimental investigations has an ultimate sensitivity of 2 parts in 10^7 or better and has been described in detail elsewhere.[29] Briefly, the laser output is split into three components, and three Princeton EG&G model 3502 lock-in amplifiers provide the capability of first or second derivative detection of the absorption at effectively up to 1.2 MHz. In the previous studies, the diode was tunable over the range 2460−2685 cm^{-1} with typical single mode scan lengths of 2−3 cm^{-1} and selected single mode power of >0.25 mW. For the current experiments, a lead salt diode supplied by Laser Analytics Inc. (Boston, MA) and centered to operate in the range of 2560−2585 cm^{-1} was installed in the spectrometer and had an estimated instrumental line width of 30 MHz. Upon completion of a frequency scan, the simultaneously digitized data from three signal channels, (i) the internally coupled Fabry−Perot interferomer (icFPI) with a free spectral range (FSR) of 0.00962456(10) cm^{-1} for relative frequency determination, (ii) a reference gas cell for absolute frequency calibration, and (iii) that directed through the supersonic expansion, are stored on the computer hard disk. Absolute transition frequencies were determined with estimated accuracies of ±0.001 cm^{-1} and generated using the reference standard[30] N_2O maintained at a pressure of 1 mTorr in the 20 cm reference cell. All signals were initially produced from matched InSb detectors with a rise time of approximately 700 ns and a $D^* = 1.6 \times 10^{11}$ cm Hz$^{1/2}$ W^{-1}. The associated amplifying electronics and detector chip responsivity and size were selected to optimize the second derivative signal from the third lock-in as well as the tuning characteristics of the lead salt diode. Data analysis involves the process of importing the data into Grams/386 where it is linearized and calibrated. Custom produced programs have been written in Array Basic for these purposes and for the subsequent spectroscopic analysis.

An adjustable stainless steel slit for generating the supersonic expansion is similar in construction to that used previously.[31] The exit length has been extended to 12.7 cm, and the width is typically adjusted to 25−50 μm. Design of the vacuum chamber has been modified to allow the calcium fluoride windows to be mounted at the Brewster angle with respect to the incident laser beam. The composition of the reservoir gas was adjusted to 1% HBr in an Ar carrier, and the spectrometer was used with a typical total stagnation pressure of 5−10 psig, argon as the carrier, and the chamber pumped to a pressure of 700−950 mTorr by a 2300 cfm Leybold-Heraeus Roots blower backed by a SV630 rotary vane pump. The diode laser output beam is focused to less than 2 mm beam waist by a CaF_2 lens with 1 m focal length. A single pass of this beam was directed through the slit expansion at a distance centered at approximately 4 mm from the opening of the slit so that its cross section matched that of the supersonic expansion.

For static gas-phase studies, a variable path length temperature controllable corrosion resistant White cell was used at typical total gas pressure of 15 Torr at −40 °C with an effective path length of 72 m. The temperature of the cell was adjusted from −30 to −50 °C to optimize the recording of lower or higher J transitions as desired. An initial equilibrium mixture consisted of HBr and Ar at room temperature in the ratio 1:5. This was subsequently slowly cooled down to the final temperature used in recording of the spectrum over a period of 3−4 h to prevent condensation on the multireflection mirrors.

Determination of the J dependence of natural line width broadening from the second derivative line profiles of the ν_1 vibration of Ar−HBr reduces to a mathematical problem which is an inverse problem of determining the three parameters a, A, and Γ given for the intensity function[32]

$$I(\omega) = A \int_0^\infty \frac{e^{-a(\omega_0-\omega')^2}}{(\omega-\omega')^2 + (\Gamma/2)^2}\, d\omega' \qquad (1)$$

From measured data corresponding to values of its second derivative function

$$\Phi(\omega) = \frac{d^2}{d\omega^2} I(\omega) \qquad (2)$$

straightforward differentiation of eq 1 leads to the expression

$$\frac{d^2}{d\omega^2} I(\omega) = \Phi(\omega) = 2A \int_0^\infty \frac{e^{-a(\omega_0-\omega')^2}(3(\omega-\omega')^2 - (\Gamma/2)^2)}{((\omega-\omega')^2 + (\Gamma/2)^2)^3}\, d\omega' \qquad (3)$$

However, the inverse problem for a, A, and Γ cannot be solved directly from eq 3 for several reasons. First, this is an

ill-posed problem, since an infinite number of sets of values for the parameter triple (a, A, Γ) will fit given values of the intensity function or its second derivative equally well. Second, the integral in eq 3 is difficult to evaluate numerically with sufficient accuracy. Finally, the expected values of the three parameters (a, A, Γ) differ by many orders of magnitude, making the inverse problem badly ill-conditioned.

The ill-posed nature of the inverse problem can be circumvented by reducing the number of parameters that must be fit. Parameter A can avoid being fit by first observing that the function $\Phi(\omega)$ has a double minimum profile and gleaning a reasonable estimate of the frequency difference between the two minima from the spectral traces. Moreover, one can determine reasonable approximations for the Gaussian spread parameter a. The single remaining parameter Γ can then be fit quite accurately from the data. We computed the intergral in eq 3 accurately and made solving the inverse problem well-conditioned by defining new, appropriately scaled parameters and performing a change of variables in the integral. Specifically, it proves convenient to define the new parameters (α, β, r) and the variable X by

$$\alpha = a\omega_0 10^{-10}$$

$$\beta = (\omega_0/\Gamma)^2 10^{-10}$$

$$r = \frac{2A\omega_0}{\Gamma^4 10^5}$$

$$X = \left(\frac{\omega}{\omega_0} - 1\right)10^5 \tag{4}$$

After a sequence of changes of variables, the integral expression for $\Phi(\omega)$ in eq 3 becomes

$$\phi(X) = \Phi(\omega) = 16\Gamma \int_{-10^5}^{\infty} \frac{e^{-\alpha p^2}(12\beta(X-p)^2 - 1)}{(4\beta(X-p)^2 + 1)^3}\,\mathrm{d}p \tag{5}$$

The integral in eq 5 is well-behaved and can be accurately evaluated numerically. To that end, the Mathematica software package[33] was used to carry out all of the required computations. Since the location of the minima in the graph of $\phi(X)$ is independent of Γ, and the value of α may be assumed to be known to within required accuracy, the value of β is then uniquely and accurately determined from eq 5 and the minima separation gleaned from the measured data. The value of r is the determined from eq 4.

III. Theoretical Calculations

Although we have studied the Ar−HBr system previously,[11,12,20] we have computed new ab initio potential energy surfaces (AIPESs) to form the basis of our morphing procedure in addition to using our previous AIPESs. In our earlier studies, the nonrelativistic interaction energies of the Ar−HBr complex were calculated using MP2 with 6-311++G(3df, 3pd) basis sets using the GAUSSIAN electronic structure package.[34] A grid of 560 (R, θ, r) points was calculated with the HBr bond distance, r, which was varied using the 8 point grid 1.2143, 1.2643, 1.3143, 1.4143, 1.55, 1.6, 1.65, and 1.7 Å, with 10 equally spaced points between 3.1932 and 5.4432 Å along the Ar−Br distance, R, and 7 equally spaced points between 0 and 180° along the H−Br−Ar angle, θ. This original potential will be referred to as the MP2 Pople (MP2P) potential. New potentials were computed using a denser grid of points, an augmented correlation consistent valence triple-ζ (aug-cc-pVTZ) basis set,[35−37] and both MP2 and CCSD(T). These two AIPESs will be referred to as the MP2CC and CCCC potentials and were computed using the MOLPRO suite of quantum chemistry codes.[38] The MP2CC and CCCC potentials were computed at 11 values of the HBr bond length with the values of r evenly spaced starting with $r = 1.2$ Å and ending with $r = 1.7$ Å. It should be noted that the equilibrium value of HBr is[39] $r_e = 1.41447$ Å. There were 13 values of the distance between the Ar and Br atoms considered, $R = 3.0$, 3.25, 3.5, 3.75, 4.0, 4.25, 4.5, 4.75, 5.0, 5.5, 6.0, 7.0, and 8.0 Å, and there were 13 evenly spaced values of the angle θ (H−Br−Ar) considered, starting with $\theta = 0°$ and ending with 180°. Thus, there were a total of $M = 1859$ points calculated. The interaction energies were then corrected for the basis set superposition error (BSSE) using the counterpoise (CP) method of Boys and Bernardi.[40]

Finally, a full BSSE corrected 3D PES was obtained by using

$$V(R,\theta,r) = V^{\mathrm{int}}(R,\theta,r) + V^{\mathrm{HBr}}(r) \tag{6}$$

where $V^{\mathrm{int}}(R,\theta,r)$ is the BSSE corrected interaction energy and $V^{\mathrm{HBr}}(r)$ is the interatomic potential for the isolated HBr molecule. In this study, we have taken $V^{\mathrm{HBr}}(r)$ to be a 1D Morse potential[41] with the parameters[42] $2\beta = 2.311216$, $D = 38796.63$ cm^{-1}, and $r_e = 1.414436$ Å. All calculations presented in this study are for complexes and monomers containing the ^{79}Br isotope. With the Morse potential given here, the fundamental transition energy for the H^{79}Br monomer is the same as the experimental value[42] of 2558.9 cm^{-1}.

Computed interaction energies were fitted to an analytical form using a three-dimensional interpolation function based on the Hilbert space reproducing kernel (HSRK) of Ho and Rabitz.[43] The approach is very similar to the method we used in our earlier study of the 3D potential of Ar−HBr.[12] In that earlier study, we used a smoothed version of the HSRK. In those potentials, we found weak oscillations in the potential that resulted from the smoothing. Thus, in the current application, we have removed the smoothing, that is, set the switching range Δx to zero. The potential is not fit directly, instead we use a transformed potential of the form[12,44]

$$\bar{V}(R,\theta,r) = \ln\left\{\frac{V(R,\theta,r) - V_{\mathrm{lower}}}{-V_{\mathrm{lower}}}\right\} \tag{7}$$

This logarithm transformation has been introduced here since it leads to a better representation when the ab initio potential is extrapolated to small R values using the reproducing kernel Hilbert space approach which is known to have a poor extrapolation behavior at small R values when using the standard implementation.[45]

The rovibrational states were then computed using the variational method previously described in detail.[12,20,46,47] In this approach, the HBr stretching motion is adiabatically separated from the bending and stretching motion of the complex. Thus at each value of R and θ, the HBr energy of the HBr (v_1) stretching state $E_{v1}(R,\theta)$ is determined. This energy then becomes the potential for the determination of the bending and stretching motion of the molecule. The intermolecular rovibrational wave function is computed using a space-fixed frame with the radial function expanded in a distributed Gaussian basis set and the angular function expanded in a coupled angular basis set. The distributed Gaussian basis set consisted of 50 functions evenly distributed from $R = 2.700$ to 6.600 Å, and the angular basis set contained an expansion of the rotational wave function

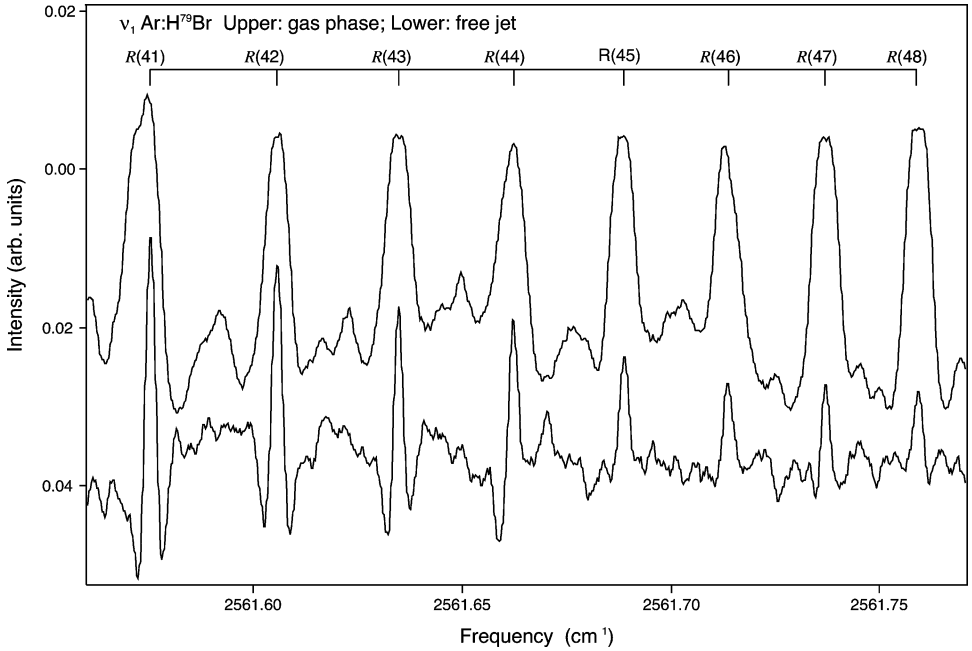

Figure 1. Rovibrational spectrum of υ_1 Ar−H^{79}Br including $R(41)$ to $R(48)$ recorded from 2561.55 to 2561.80 cm^{-1} in a supersonic slit jet (lower trace) and static gas-phase mixture (upper trace).

of the HBr monomer using states up to $j_{max} = 14$. All possible end-over-end rotational states were included consistently with this value of j_{max} and the value of the total angular momentum of a given state. The rovibrational states are computed in two steps. First, a vibrational self-consistent field (VSCF) calculation is performed in which the angular state is computed in an angular potential obtained from the full intermolecular potential by averaging over the ground radial vibrational state. The radial state is obtained from a 1D vibrational calculation where the potential is obtained from the full intermolecular potential by averaging over the bending state. The VSCF equations are solved iteratively. Converged VSCF bending and stretching wave functions are then combined in a direct product basis set which is used in a vibrational configuration interaction (VCI) calculation for the final rovibrational states. In the morphing procedure discussed below, the derivatives of the rovibrational eigenvalues with respect to the morphing parameters are used. These derivatives are computed using the Hellmann−Feynman theorem. Rotational constants used for the diatomic molecules in the complex were the estimated values at the minimum of the adiabatic potential:[12] 8.35789 cm^{-1} for H^{79}Br ($\upsilon = 0$), 8.14383 cm^{-1} for H^{79}Br ($\upsilon = 1$), and 4.25008 cm^{-1} for D^{79}Br ($\upsilon = 0$).

The ab initio potential, $V_{\text{ab initio}}(R,\theta,r)$, is morphed using the transformation

$$V_{\text{morphed}}(R,\theta,r) = S_1(\theta,r)V_{\text{ab initio}}(S_2(\theta,r)(R - R_F) + [1 + S_3(\theta,r)]R_F,\theta,r) \quad (8)$$

where

$$S_\alpha(\theta,r) = \sum_{i,j} C_{\alpha,i,j}P_i(\cos\theta)\left[1 - \exp\left(-\beta\frac{r - r_e}{r_e}\right)\right]^j \quad (9)$$

We note that all of the morphing parameters $C_{\alpha,i,j}$ are numbers without units. In the present study, R_F was taken to be 3.94 Å and β was taken to be 1.0. The values of the morphing parameters were obtained by a regularized nonlinear least-squares optimization. In the regularized procedure,

TABLE 1: Fitted Lorentzian Linewidth (fwhm) Γ of ν_1 Ar−HBr Spectral Lines that Are Not Predissociatively Broadened

ν_1 Ar−H^{79}Br transition	Γ (MHz)	ν_1 Ar−H^{81}B transition	Γ (MHz)
$P(13)$	369(9)	$P(38)$	354(34)
$P(23)$	378(9)	$P(51)$	356(34)
$P(48)$	362(9)	$P(56)$	359(34)
$R(42)$	359(9)	$P(70)$	319(34)
$R(45)$	372(9)	$P(74)$	357(34)
$R(48)$	366(9)	$P(75)$	392(34)
$\bar{\Gamma}$	367(11)	$\bar{\Gamma}$	356(36)

the function that is minimized is

$$F(C_{\alpha,i,j},\gamma) = \sum_{k=1}^{M}\left\{\frac{O_k^{\text{expt}} - O_k^{\text{calc}}(C_{\alpha,i,j})}{\sigma_k}\right\}^2 + \gamma^2\sum_{\alpha,i,j}(C_{\alpha,i,j} - C_{\alpha,i,j}^0)^2 \quad (10)$$

where O_k^{expt} values are experimentally observed quantities, O_k^{calc} values are the corresponding calculated quantities, γ is the regularization parameter, σ_k values are the uncertainties in either the observed or computed values, and $C_{\alpha,i,j}^0$ are the values of the morphing parameters which correspond to no morphing, that is, $C_{1,0,0}^0 = 1, C_{2,0,0}^0 = 1$, and all others are zero. All calculated quantities, O_k^{calc}, are obtained by finite difference as described in our earlier study.[12] Minimizing F then yields a potential that simultaneously improves the agreement between the experimental and calculated observables and keeps the morphed potential close to the original ab initio potential. The quality of the fit of the experimental data can then be characterized by the root-mean-square deviation from the experimental data

$$G(\gamma) = \left[\frac{1}{M}\sum_{k=1}^{M}\left\{\frac{O_k^{\text{expt}} - O_k^{\text{calc}}(C_{\alpha,i,j})}{\sigma_k}\right\}^2\right]^{1/2} \quad (11)$$

In eq 11, the value of G depends on the value of γ since the

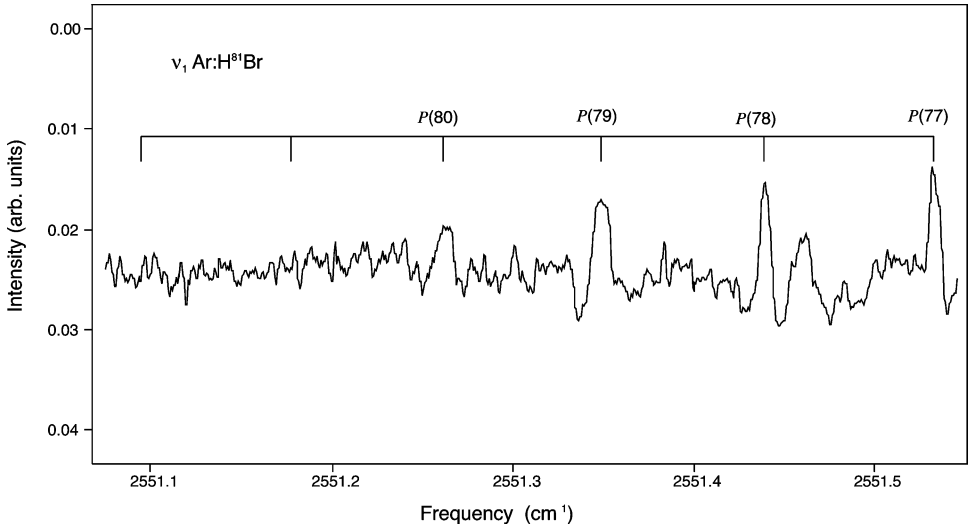

Figure 2. Rovibrational spectrum of $P(77)$ to $P(80)$ ν_1 Ar−H^{81}Br recorded from 2551.07 to 2551.54 cm^{-1} in a static gas-phase mixture with an effective absorption path length of 72 m. The spectrum illustrates the effect of predissociative line broadening and the inability to detect the $P(81)$ and $P(82)$ transitions of the isotopomer using this spectroscopic method.

morphing parameters $C_{\alpha,i,j}$ depend implicitly on γ through the minimization of F given in eq 10. Note that $G(\gamma=\infty)$ is the deviation from the experimental data of the observables predicted from the ab initio potential energy surface (i.e., the unmorphed surface).

There is a direct connection between the type of available experimental data and the morphing parameters that can be determined. Rotation constants are most sensitive to the $C_{3,i,j}$ morphing parameters which shift the potential. Distortion constants are sensitive to the curvature of the potential in the radial direction which is controlled by the overall scaling parameters $C_{1,i,j}$ and the radial dilation parameters $C_{2,i,j}$. The values of $\langle P_2(\cos\theta)\rangle$, the energy difference between the Ar−HBr and Ar−BrH vibrational states, and the frequency of the bending mode are sensitive to the overall scaling parameters $C_{1,i,j}$.

We have also estimated the uncertainty in the morphed potential by considering the sensitivity of the values of the potential to the quality of the fit. Using the same approach as in our previous work,[12] the computed uncertainties represent the root-mean-square difference in the potential between the optimized value and the value of the potential where the parameters are on the boundary of the confidence region with[48] $\Delta\chi^2 = \chi^2_{\min}$. The values of the potential used in the uncertainty estimate were relative to the value at infinite separation.

The value of D_0 was estimated using a 1D model for the lifetimes of the high J states of Ar−HBr. The 1D potential used, $V_{1D}(R)$, was obtained by computing the average over θ of the $\upsilon = 0$ adiabatic potential of Ar−H^{79}Br determined previously.[11] This potential was then morphed to fit the lifetime data determined from the analysis of the experimental line shapes. The morphing transformation was similar to that used to fit the full potential and was of the form

$$V^{(\upsilon)}_{1D,\text{morphed}}(R) = S^{(\upsilon)}_{1D,1} V_{1D}(S^{(\upsilon)}_{1D,2}(R - R_{1D,F}) + (1 + S^{(\upsilon)}_{1D,3})R_{1D,F}) \quad (12)$$

where $R_{1D,F}$ was taken to be 4.2 Å, which is near the minimum in the unmorphed V_{1D} and where the superscript υ indicates the vibrational state of the HBr monomer for the particular adiabatic 1D potential. For a given choice of morphing parameters for the lower ($\upsilon = 0$) and upper states ($\upsilon = 1$), the lifetimes of the various J states were obtained by solving the radial scattering equation

$$-\frac{\hbar^2}{2\mu}\frac{d^2 f_{J,\upsilon}(R)}{dR^2} + \frac{\hbar^2 J(J+1)}{2\mu R^2} f_{J,\upsilon}(R) + V^{(\upsilon)}_{1D,\text{morphed}}(R) f_{J,\upsilon}(R) = E f_{J,\upsilon}(R) \quad (13)$$

and obtaining the corresponding S matrix as a function of the energy E. The resonant states occur where the S matrix has a pole at complex energy $E = E_{R,J,\upsilon} - i\Gamma_{J,\upsilon_1}/2$. The intrinsic width of a particular $P(J)$ was then taken to be $\Gamma(P(J)) = \Gamma_{J,\upsilon_1=0} + \Gamma_{J-1,\upsilon_1=1}$.

TABLE 2: Fitted Lorentzian Linewidth (fwhm) Γ of ν_1 Ar−HBr Predissociation-Broadened Spectral Lines

ν_1 Ar−H^{79}Br transition	Γ(MHz)	$\Gamma - \bar{\Gamma}$ (MHz)	ν_1 Ar−H^{81}Br transition	Γ (MHz)	$\Gamma - \bar{\Gamma}$ (MHz)
$P(78)$	462(18)	95(29)	P(78)	459(9)	103(45)
$P(79)$	592(24)	225(35)	P(79)	582(11)	226(47)
$P(80)$	1027(41)	660(52)	P(80)	1087(19)	731(55)

TABLE 3: Computed Energies and Widths of the High J States with $\upsilon_2 = 0$ and $\upsilon_3 = 0$ for the 1D Model of Ar−H^{79}Br

υ_1	J	E/(cm^{-1})	Γ/(MHz)
0	78	83.54	24.30
0	79	88.52	126.05
0	80	93.52	499.45
0	81	98.50	1758.23
1	77	76.53	7.36
1	78	81.39	48.55
1	79	86.27	226.99
1	80	91.13	957.19
1	81	95.99	2912.57

IV. Results and Discussion

The supersonic jet spectra of ν_1 Ar−HBr were recorded from $P(52)$ to $R(59)$ at an effective temperature of approximately 12 K as determined from rovibrational intensity distributions. Transitions for $R(41)$ to $R(48)$, 2561.55−2561.80 cm^{-1}, are shown in Figure 1. Frequencies of these transitions have been measured and combine with measured frequencies for higher transitions recorded in static gas-phase spectra to determine the

TABLE 4: Experimental Observables and Their Corresponding Computed Values Used To Morph the Ar−HBr PES for All Three Calculations Considered

	unmorphed			morphed					
observable	MP2P	MP2CC	CCCC	MP2P	MP2CC	CCCC	O_k^{expt}	exp[a]	σ
Ar−HBr D_0/cm^{-1}	84.2	117.9	94.7	129.2	129.9	129.9	130.	(A)	1
Ar−HBr $\{E[(0,2^0,0)_1] - E[(0,0^0,0)_0]\}$/cm^{-1}	13.55	16.10	17.13	11.05	11.12	10.98	11.08	(B)	0.04
Ar−HBr $\{E[(0,1^{-1},0)_1] - E[(0,0^0,0)_1]\}$/cm^{-1}	26.71	32.19	28.05	26.63	26.56	26.67	26.67	(B, C)	0.04
Ar−HBr $\{E[(1,0^0,0)_0] - E[(0,0^0,0)_0]\}$/cm^{-1}	−0.795	−1.472	0.430	0.334	0.340	0.341	0.337	(B)	0.013
Ar−HBr $\{E[(1,2^0,0)_1] - E[(1,0^0,0)_0]\}$/cm^{-1}	13.089	15.704	15.738	9.322	9.283	9.341	9.280	(B)	0.023
Ar−HBr $\{E[(1,1^1,0)_1] - E[(1,0^0,0)_1]\}$/cm^{-1}	26.48	32.28	26.92	25.47	25.64	25.49	25.47	(B)	0.05
Ar−HBr $\{E[(1,1^{-1},0)_1] - E[(1,0^0,0)_1]\}$/cm^{-1}	26.48	32.28	26.92	25.47	25.64	25.49	25.47	(B)	0.05
Ar−HBr $\{E[(1,0^0,1)_1] - E[(1,0^0,0)_0]\}$/cm^{-1}	21.45	26.32	23.57	25.76	25.91	25.78	25.75	(B)	0.12
Ar−HBr $\{E[(1,2^0,1)_1] - E[(1,0^0,0)_0]\}$/cm^{-1}	30.74	36.68	34.31	31.81	31.76	31.73	31.73	(B)	0.11
Ar−HBr $B[(0,0^0,0)_{1,0}]$/ (0.01 cm^{-1})	3.466	3.571	3.472	3.690	3.694	3.689	3.691	(D, E)	0.004
Ar−HBr $B[(0,2^0,0)_{1,0}]$/(0.01 cm^{-1})	3.6273	3.9712	3.7470	4.1242	4.1238	4.1243	4.1238	(B)	0.0004
Ar−HBr $B[(0,1^{-1},0)_{2,1}]$/(0.01 cm^{-1})	3.498	3.665	3.553	3.822	3.822	3.814	3.813	(B, C)	0.003
Ar−HBr $B[(1,0^0,0)_{1,0}]$/(0.01 cm^{-1})	3.443	3.535	3.436	3.652	3.654	3.670	3.664	(B)	0.005
Ar−HBr $B[(1,2^0,0)_{1,0}]$/(0.01 cm^{-1})	3.6337	3.9859	3.7480	4.1256	4.1259	4.1255	4.1256	(B)	0.0004
Ar−HBr $B[(1,1^1,0)_{2,1}]$/(0.01 cm^{-1})	3.530	3.655	3.579	3.740	3.738	3.741	3.744	(B)	0.004
Ar−HBr $B[(1,1^{-1},0)_{2,1}]$/(0.01 cm^{-1})	3.498	3.654	3.542	3.798	3.802	3.808	3.803	(B)	0.004
Ar−HBr $B[(1,0^0,1)_{2,1}]$/(0.01 cm^{-1})	3.265	3.413	3.286	3.648	3.649	3.652	3.677	(B)	0.008
Ar−HBr $B[(1,2^0,1)_{1,0}]$/(0.01 cm^{-1})	3.5006	3.8129	3.6093	3.9276	3.9275	3.9277	3.9275	(B)	0.0008
Ar−DBr $B[(0,0^0,0)_{1,0}]$/(0.01 cm^{-1})	3.424	3.541	3.441	3.627	3.626	3.621	3.627	(D, E)	0.003
Ar−HBr $D[(0,0^0,0)_{2,1,0}]$/(1.0 × 10^{-7} cm^{-1})	3.63	2.73	3.14	4.24	4.15	4.23	4.14	(D, E)	0.04
Ar−HBr $D[(0,2^0,0)_{2,1,0}]$/(1.0 × 10^{-7} cm^{-1})	5.10	5.19	6.28	4.15	4.18	4.15	4.10	(B)	0.04
Ar−HBr $D[(0,1^{-1},0)_{3,2,1}]$/(1.0 × 10^{-7} cm^{-1})	4.36	3.47	3.84	3.54	3.49	3.47	3.61	(B, C)	0.05
Ar−HBr $D[(1,0^0,0)_{2,1,0}]$/(1.0 × 10^{-7} cm^{-1})	3.70	2.71	3.32	5.37	5.35	5.37	5.17	(B)	0.05
Ar−HBr $D[(1,2^0,0)_{2,1,0}]$/(1.0 × 10^{-7} cm^{-1})	5.13	5.29	6.36	3.23	3.19	3.20	3.24	(B)	0.04
Ar−HBr $D[(1,1^{-1},0)_{3,2,1}]$/(1.0 × 10^{-7} cm^{-1})	4.31	3.49	3.87	3.57	3.60	3.56	3.54	(B)	0.05
Ar−HBr $D[(1,2^0,1)_{2,1,0}]$/(1.0 × 10^{-7} cm^{-1})	6.12	5.97	5.88	3.81	3.78	4.02	3.68	(B)	0.11
Ar−DBr $D[(0,0^0,0)_{2,1,0}]$/(1.0 × 10^{-7} cm^{-1})	2.98	2.30	2.65	2.89	2.81	2.87	2.83	(D, E)	0.04
Ar−HBr $\langle P_1(\cos\theta')\rangle$ for $(0,0^0,0)_0$	0.61	0.72	0.67	0.61	0.61	0.61	0.60	(F)	0.03
Ar−DBr $\langle P_1(\cos\theta')\rangle$ for $(0,0^0,0)_0$	0.84	0.84	0.82	0.80	0.80	0.79	0.80	(F)	0.04
Ar−HBr $\langle P_2(\cos\theta')\rangle$ for $(0,0^0,0)_0$	0.3526	0.4292	0.3589	0.3261	0.3250	0.3264	0.3254	(D, E)	0.0005
Ar−HBr $\langle P_2(\cos\theta')\rangle$ for $(0,2^0,0)_0$	0.422	0.464	0.382	0.494	0.490	0.488	0.490	(G)	0.002
Ar−HBr $\langle P_2(\cos\theta')\rangle$ for $(0,1^{-1},0)_1$	−0.142	−0.060	−0.095	−0.095	−0.098	−0.093	−0.098	(B, C)	0.002
Ar−DBr $\langle P_2(\cos\theta')\rangle$ for $(0,0^0,0)_0$	0.6122	0.6080	0.5537	0.5217	0.5210	0.5172	0.5206	(D, E)	0.0015
Ar−HBr $D_\theta^{(1,0)}/10^{-6}$ for $(0,0^0,0)$	15.3	14.8	17.6	33.5	33.9	33.2	34.6	(D, E)	0.5
Ar−HBr $D_\theta^{(1,0)}/10^{-6}$ for $(0,2^0,0)$	−57.3	−52.7	−65.8	−59.9	−60.3	−61.0	−59.6	(G)	0.7
Ar−DBr $D_\theta^{(1,0)}/10^{-6}$ for $(0,0^0,0)$	14.3	10.6	14.1	28.0	29.0	27.9	27.8	(D, E)	0.8
χ	317.13	122.7	247.6	1.49	1.63	1.71			

[a] Source of experimental data: (A), this paper; (B), ref 20; (C), ref 50; (D), ref 51; (E), ref 52; (F), ref 5; (G), ref 11.

more accurate rovibrational parameters given below, where the parameters have been fitted to

$$v = v_0 + E(J') - E(J'') \tag{14}$$

where

$$E_v(J) = B_vJ(J+1) - D_JJ^2(J+1)^2 + H_vJ^3(J+1)^3 + L_vJ^4(J+1)^4 + M_vJ^5(J+1)^5 + P_vJ^6(J+1)^6 \tag{15}$$

The fits gave for ν_0, B_v'', D_J'', H_v'', L_v'', M_v'', P_v'', values of Ar−H^{81}Br: 2558.86904(12), 3.6611394(2) × 10^{-2}, 4.1034(14) × 10^{-7}, 4.67(13) × 10^{-11}, −1.150(101) × 10^{-14}, 1.30(27) × 10^{-18}, −6.43(25) × 10^{-23} and B_v', D_J', H_v', L_v', M_v', P_v', 3.633927(78) × 10^{-2}, 5.055(14) × 10^{-7}, 7.95(15) × 10^{-11}, −1.82(10) × 10^{-14}, 2.02(29) × 10^{-18}, −9.24(27) × 10^{-23} cm^{-1}, respectively. In the case of Ar−H^{79}Br, the corresponding constants are in the ground state: 2559.25031(12), 3.6914578(2) × 10^{-2}, 4.1702(12) × 10^{-7}, −0.855(28) × 10^{-14}, 0.740(51) × 10^{-18}, −3.61(30) × 10^{-23} and in the excited state, 3.663888(81) × 10^{-2}, 5.098(14) × 10^{-7}, 7.25(11) × 10^{-11}, −1.420(44) × 10^{-14}, 1.261(71) × 10^{-18}, −5.23(41) × 10^{-23} cm^{-1}. The standard deviations of the fits for Ar−H^{81}Br is $\sigma = \pm 0.00046$ cm^{-1} and for Ar−H^{79}Br, $\sigma = \pm 0.00052$ cm^{-1}.

Fitted Lorentzian full widths at half-maximum (fwhm) were evaluated as described in section II, and a range of selected results are given as part of Table 1. As can be seen, the determined line widths are within two standard deviations of the fitted fwhm for each transition; there is no significant rotational dependence of the line width for transitions investigated in the static gas-phase studies with an average value of 367(11) MHz.

TABLE 5: Optimized Morphing Parameters $C_{\alpha,i,j}$ and Their Corresponding Uncertainties

	MP2P		MP2CC		CCCC	
(α,i,j)	$C_{\alpha,i,j}$	σ	$C_{\alpha,i,j}$	σ	$C_{\alpha,i,j}$	σ
(1,0,0)	1.5360	0.0113	1.1602	0.0085	1.4039	0.0100
(1,1,0)	0.0141	0.0025	−0.0061	0.0018	−0.0545	0.0021
(1,2,0)	−0.0951	0.0070	−0.0888	0.0028	−0.0779	0.0028
(1,3,0)	−0.1178	0.0029	−0.0457	0.0022	−0.0503	0.0025
(1,4,0)	−0.0835	0.0086				
(1,0,1)	−0.1619	0.0204	−0.1727	0.0156		
(2,0,0)	1.0128	0.0066	0.9875	0.0060	0.9847	0.0059
(2,1,0)	0.0452	0.0066	0.0669	0.0058	0.0484	0.0057
(2,2,0)	−0.1069	0.0204	0.0522	0.0097	−0.0021	0.0057
(2,3,0)	0.0116	0.0132	−0.0650	0.0090	−0.0857	0.0086
(2,4,0)	0.2751	0.0305	−0.1353	0.0198		
(3,0,0)	0.0491	0.0003	0.0214	0.0002	0.0358	0.0002
(3,1,0)	−0.0223	0.0005	−0.0053	0.0003	−0.0077	0.0003
(3,2,0)	−0.0205	0.0009	−0.0135	0.0006	−0.0096	0.0006
(3,3,0)	0.0122	0.0014				
(3,0,1)	−0.0700	0.0029	−0.0470	0.0025	0.0222	0.0024
(3,1,1)	−0.0719	0.0042	−0.0455	0.0041	0.0142	0.0027

TABLE 6: Correlation Matrix of the Morphing Parameters, $C_{\alpha,I,j}$ for the Morphed CCCC Potential

(α,*i*,*j*)	(1,0,0)	(1,1,0)	(1,2,0)	(1,3,0)	(2,0,0)	(2,1,0)	(2,2,0)	(2,3,0)	(3,0,0)	(3,1,0)	(3,2,0)	(3,0,1)	(3,1,1)
(1,0,0)	1.00												
(1,1,0)	−0.54	1.00											
(1,2,0)	−0.96	0.63	1.00										
(1,3,0)	0.27	−0.90	−0.39	1.00									
(2,0,0)	−0.73	0.22	0.57	−0.11	1.00								
(2,1,0)	−0.02	0.73	0.08	−0.70	−0.20	1.00							
(2,2,0)	0.31	−0.13	−0.11	0.16	−0.81	−0.03	1.00						
(2,3,0)	−0.17	−0.24	0.25	0.36	0.03	−0.70	0.32	1.00					
(3,0,0)	−0.25	0.46	0.27	−0.25	0.02	0.30	0.15	−0.04	1.00				
(3,1,0)	0.61	−0.22	−0.53	0.02	−0.68	0.29	0.40	−0.49	−0.01	1.00			
(3,2,0)	0.10	−0.79	−0.25	0.70	0.21	−0.67	−0.23	0.05	−0.60	0.09	1.00		
(3,0,1)	0.12	−0.09	−0.13	0.05	−0.07	0.14	0.00	−0.24	−0.20	0.25	0.02	1.00	
(3,1,1)	0.03	0.14	−0.05	−0.16	0.02	0.10	−0.10	−0.05	0.20	−0.19	−0.13	−0.81	1.00

TABLE 7: Correlation Matrix of the Morphing Parameters, $C_{\alpha,I,j}$ for the Morphed MP2CC Potential

(α,*i*,*j*)	(1,0,0)	(1,1,0)	(1,2,0)	(1,3,0)	(1,0,1)	(2,0,0)	(2,1,0)	(2,2,0)	(2,3,0)	(2,4,0)	(3,0,0)	(3,1,0)	(3,2,0)	(3,0,1)	(3,1,1)
(1,0,0)	1.00														
(1,1,0)	−0.47	1.00													
(1,2,0)	−0.94	0.60	1.00												
(1,3,0)	0.32	−0.92	−0.49	1.00											
(1,0,1)	−0.29	0.30	0.31	−0.17	1.00										
(2,0,0)	−0.73	0.16	0.55	−0.12	0.19	1.00									
(2,1,0)	0.00	0.72	0.07	−0.67	−0.05	−0.20	1.00								
(2,2,0)	0.04	0.18	0.26	−0.22	0.04	−0.46	0.04	1.00							
(2,3,0)	−0.20	−0.24	0.23	0.33	0.19	0.08	−0.73	0.16	1.00						
(2,4,0)	0.18	−0.25	−0.41	0.33	−0.10	−0.01	−0.04	−0.82	−0.03	1.00					
(3,0,0)	−0.25	0.41	0.20	−0.17	0.28	0.08	0.25	−0.12	0.02	0.24	1.00				
(3,1,0)	0.53	−0.18	−0.54	0.14	0.13	−0.57	0.24	−0.13	−0.44	0.40	0.09	1.00			
(3,2,0)	0.10	−0.78	−0.21	0.64	−0.06	0.18	−0.65	−0.09	0.07	−0.07	−0.60	0.08	1.00		
(3,0,1)	0.11	−0.09	−0.10	0.04	−0.17	−0.06	0.15	−0.02	−0.28	0.01	−0.27	0.23	0.06	1.00	
(3,1,1)	0.16	−0.09	−0.15	−0.01	−0.70	−0.09	0.07	0.08	−0.12	−0.10	−0.08	−0.33	−0.03	−0.49	1.00

TABLE 8: Correlation Matrix of the Morphing Parameters, $C_{\alpha,I,j}$ for the Morphed MP2P Potential

(α,*i*,*j*)	(1,0,0)	(1,1,0)	(1,2,0)	(1,3,0)	(1,4,0)	(1,0,1)	(2,0,0)	(2,1,0)	(2,2,0)	(2,3,0)	(2,4,0)	(3,0,0)	(3,1,0)	(3,2,0)	(3,3,0)	(3,0,1)	(3,1,1)
(1,0,0)	1.00																
(1,1,0)	−0.34	1.00															
(1,2,0)	−0.50	−0.25	1.00														
(1,3,0)	0.12	−0.86	0.17	1.00													
(1,4,0)	−0.05	0.59	−0.76	−0.43	1.00												
(1,0,1)	−0.27	0.23	0.19	−0.06	−0.04	1.00											
(2,0,0)	−0.68	0.24	0.02	−0.07	0.30	0.17	1.00										
(2,1,0)	0.10	0.60	−0.36	−0.47	0.19	−0.05	−0.09	1.00									
(2,2,0)	−0.03	−0.38	0.80	0.17	−0.79	0.06	−0.50	−0.31	1.00								
(2,3,0)	−0.21	0.03	0.09	0.03	0.31	0.09	0.10	−0.68	−0.03	1.00							
(2,4,0)	0.14	0.26	−0.74	−0.07	0.76	−0.12	0.25	0.12	−0.89	0.30	1.00						
(3,0,0)	−0.15	0.62	−0.52	−0.29	0.69	0.19	0.27	0.33	−0.65	0.20	0.66	1.00					
(3,1,0)	0.32	−0.28	0.16	0.10	−0.14	0.05	−0.43	−0.37	0.24	0.33	0.12	−0.14	1.00				
(3,2,0)	0.03	−0.83	0.56	0.61	−0.70	0.00	−0.10	−0.58	0.59	−0.13	−0.55	−0.80	0.31	1.00			
(3,3,0)	0.06	0.47	−0.77	−0.25	0.65	0.00	0.21	0.59	−0.70	−0.34	0.45	0.55	−0.64	−0.61	1.00		
(3,0,1)	0.08	−0.18	0.09	0.10	−0.28	−0.28	−0.09	0.27	0.16	−0.53	−0.29	−0.39	−0.15	0.19	0.06	1.00	
(3,1,1)	0.12	−0.18	0.17	−0.04	−0.25	−0.64	−0.17	−0.01	0.32	−0.14	−0.34	−0.30	−0.13	0.17	−0.22	−0.16	1.00

Static gas-phase studies have enabled us to determine the frequencies of an extended range of rovibrational transitions. The corresponding transitions that do not show significant rotational predissociative line broadening are also given in Table 1 for selected representative $P(J)$ transitions given from $P(38)$ to $P(75)$ where the average value 356(36) MHz is determined. The static gas-phase spectrum corresponding to the $R(41)$ to $R(48)$ transitions in the frequency range 2561.55−2561.80 cm^{-1} are also shown in Figure 1. The $P(J)$ transitions especially of Ar−H^{81}Br are significantly less overlapped than other transitions. Transitions $P(78)$, $P(79)$, and $P(80)$ for both Ar−H^{79}Br and Ar−H^{81}Br show broadening (Figure 2) in their fitted Lorentzian line profiles (fwhm) as can also be seen in Table 2 in columns 2 and 5, and the predissociative contributions are given in columns 3 and 6 with estimated uncertainties. Γ values for transitions up to $P(75)$ do not show significant predissociative line broadening enhancement in our experiments, whether observed in supersonic jet or static gas-phase spectra, though $P(78)$, $P(79)$, and $P(80)$ transitions are significantly larger due primarily to predissociation broadening. As can be seen in Figure 2, however, we are not able to detect the $P(81)$ transition in either the ν_1 transition of Ar−H^{79}Br or Ar−H^{81}Br. The $R(J)$ branch side, although more overlapped, also gives no indication of ν_1 rovibrational transitions beyond $R(78)$ which indicates that we cannot detect transitions beyond $J = 79$ in the excited vibrational state.

Line widths were fit to obtain a value for D_0 using the 1D model discussed in the previous section. In this model, there are six adjustable parameters, three $S_{1D,i}^{(\nu_1)}$ for $\nu_1 = 0$ and three $S_{1D,i}^{(\nu_1)}$ for $\nu_1 = 1$. To reduce the number of freely adjustable parameters, the value of $S_{1D,1}^{(\nu_1=0)}$ was taken to be independent,

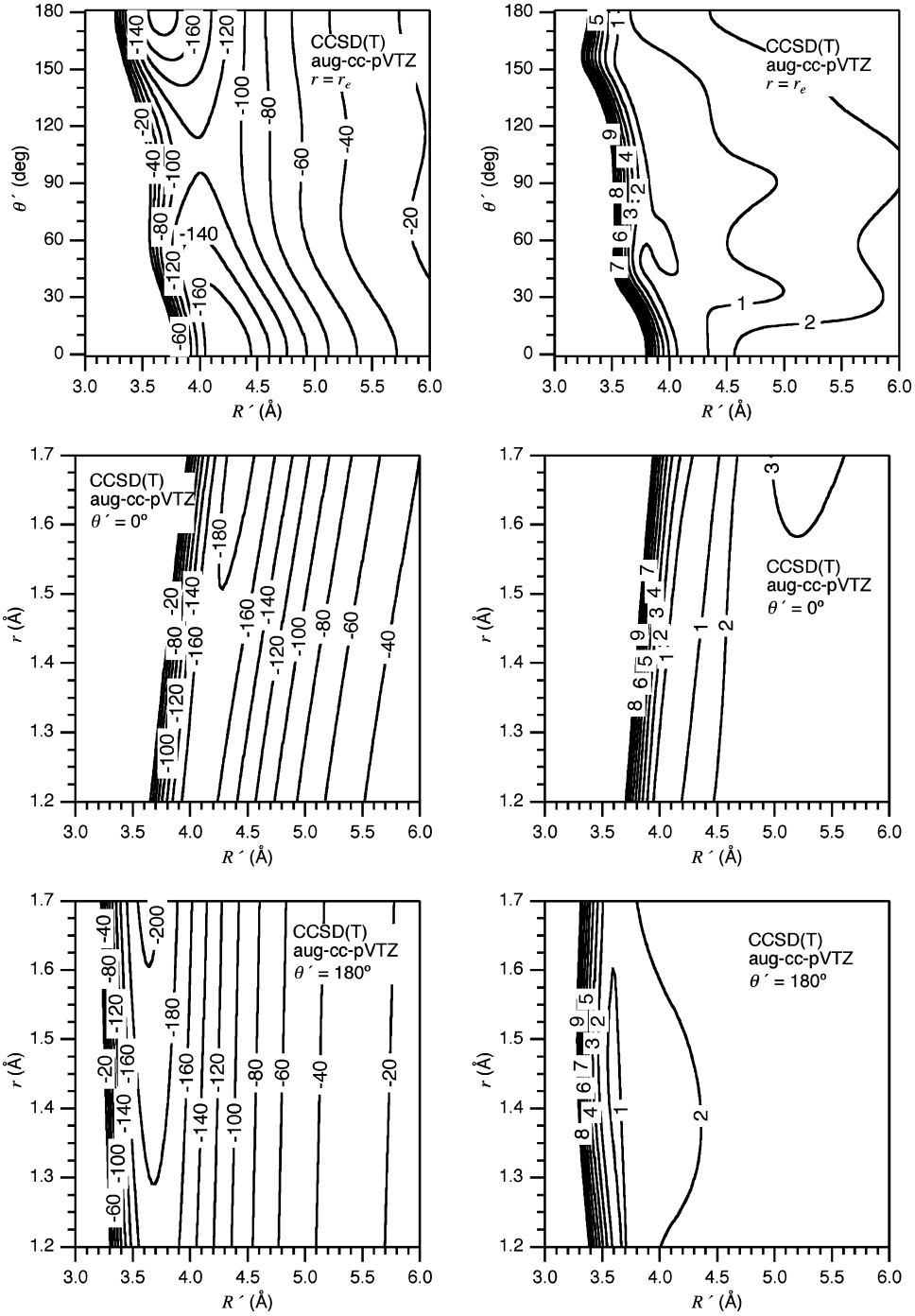

Figure 3. Morphed CCCC interaction potential of Ar−HBr. On the left side of the figure, three cuts through the 3D potential are given: $V^{\text{int}}(R',\theta',r=r_e)$, $V^{\text{int}}(R',\theta'=0°,r)$, and $V^{\text{int}}(R',\theta'=180°,r)$. The panels on the right-hand side of the figure are the corresponding statistical uncertainties in the potential relative to the potential at infinite separation of the fragments. All contours are given in cm^{-1}. The coordinates used (R',θ',r) are the Jacobi coordinates for the Ar−H^{79}Br isotopomer.

and the other five parameters were then chosen so the $\nu_3 = 26.74\ \text{cm}^{-1}$ and $B_0 = 3.691\ \text{cm}^{-1}$ for $\upsilon_1 = 0$ and $\nu_3 = 25.67\ \text{cm}^{-1}$ and $B_0 = 3.664\ \text{cm}^{-1}$ for $\upsilon_1 = 1$, with the additional constraint that $E[(1,0^0,0)_0] - E[(0,0^0,0)_0] = 0.34\ \text{cm}^{-1}$.

The value of $S_{1D,1}^{(\upsilon_1=0)}$ was then varied to obtain the best agreement with the experimentally determined line widths. The best fit to the experimental data was found for $S_{1D,1}^{(\upsilon_1=0)} = 1.3745$, $S_{1D,2}^{(\upsilon_1=0)} = 0.8792$, $S_{1D,3}^{(\upsilon_1=0)} = -0.0268$, $S_{1D,1}^{(\upsilon_1=0)} = 1.3651$, $S_{1D,2}^{(\upsilon_1=0)} = 0.8423$, and $S_{1D,3}^{(\upsilon_1=0)} = -0.0308$. In Table 3, we have given the widths and scattering energies for the resonant states for $\upsilon_1 = 0$ and $\upsilon_1 = 1$. This model then yields predicted line widths of $\Gamma(P(78)) = 31$ MHz, $\Gamma(P(79)) = 175$ MHz, and $\Gamma(P(80)) = 726$ MHz with a root-mean-square difference between the fit and the experimental weighted by the experimental uncertainties of 1.68. The experimental energy of the $\upsilon_1 = 0$, $J = 79$ state is 218.8 cm^{-1} above the $J = 0$ ground state, so that, with our computed scattering energy for this state of 88.52 cm^{-1}, this leads to an estimate of the value of $D_0 = 130 \pm 1\ \text{cm}^{-1}$. Error estimates are obtained by considering the variation of the estimated value of D_0 when the model is allowed to change so that the root-mean-square difference increases by up to a factor of 2. This value will then be used to obtain morphed potentials as discussed below.

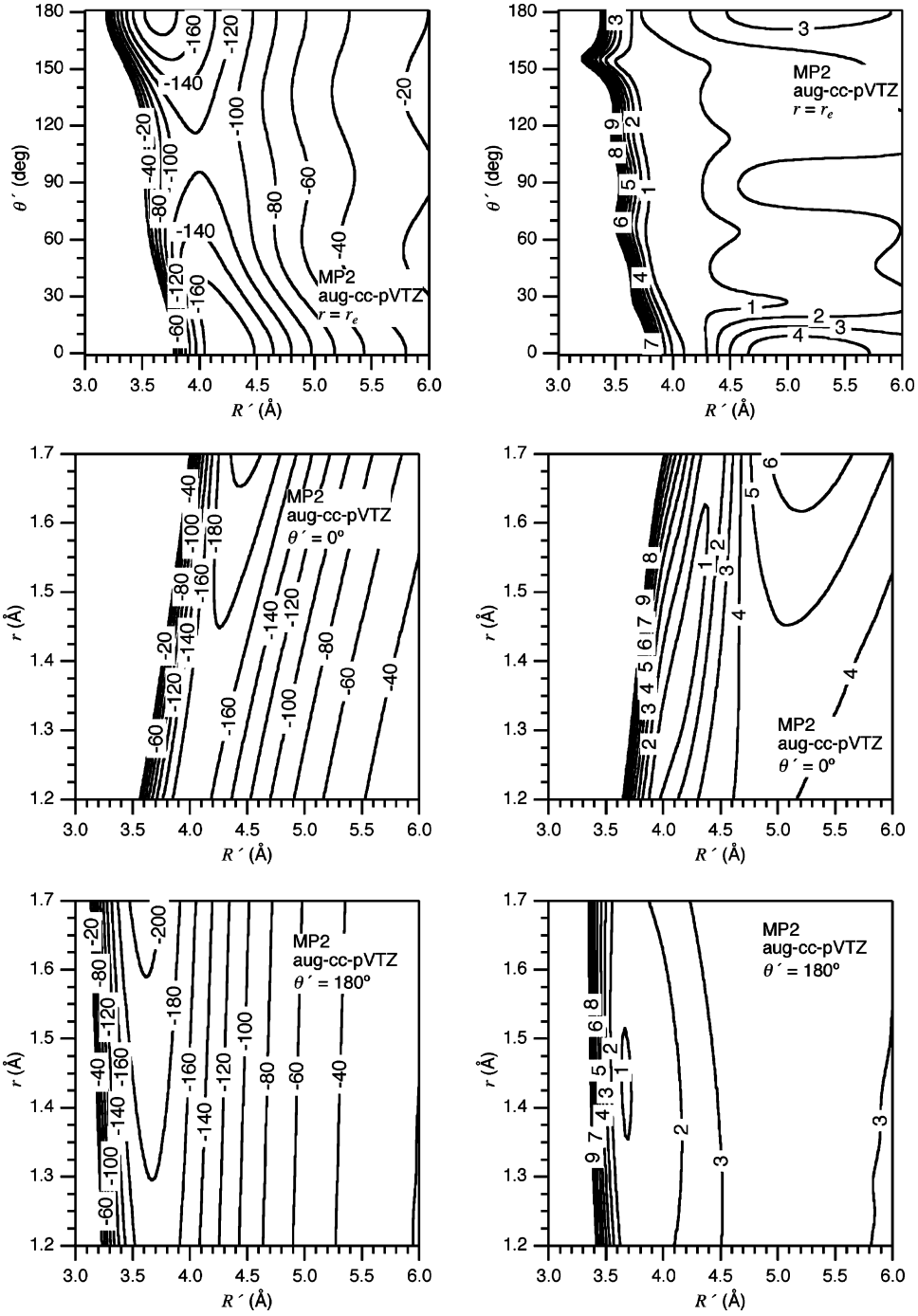

Figure 4. Morphed MP2CC interaction potential of Ar−HBr. See the caption of Figure 3 for additional details.

In Table 4, we give the predicted spectroscopic data obtained from the three AIPESs and compare those values with available experimental data, including the value of D_0 determined here. The MP2CC calculation gives the best unmorphed predictions, as judged by the value of χ, of the experimental data. This is in large part due to an approximate cancellation of errors. The MP2 treatment of correlation overestimates the binding energy of the dimer for a given basis set, and the lack of convergence in the one-electron triple-ζ basis set leads to an underestimation of the binding energy. One feature where the CCSD(T) calculation does noticeably better than either of the MP2 calculations is the frequency shift of ν_1 relative to the value for the isolated HBr molecule. As seen in Table 4, the CCSD(T) calculation gives a value of 0.430 cm^{-1} compared to the experimental value of 0.334 cm^{-1}, whereas the MP2 calculations give values with the wrong sign, -0.795 cm^{-1} for MP2P and -1.472 cm^{-1} for MP2CC.

These AIPESs were then morphed to obtain the best fit to the experimental data. The resulting spectroscopic data and the quality of fits for the three morphed potentials are also given in Table 4. The choice of morphing parameters for each potential was determined by adding parameters systematically until the value of χ was less than 1.75. When this level of convergence was obtained, the highest angular component parameters of each type were then removed one-by-one until the smallest possible set was obtained for which χ remained less than 1.75. The values of the parameters and their corresponding estimated uncertainties are given in Table 5. Values of the uncertainties and the

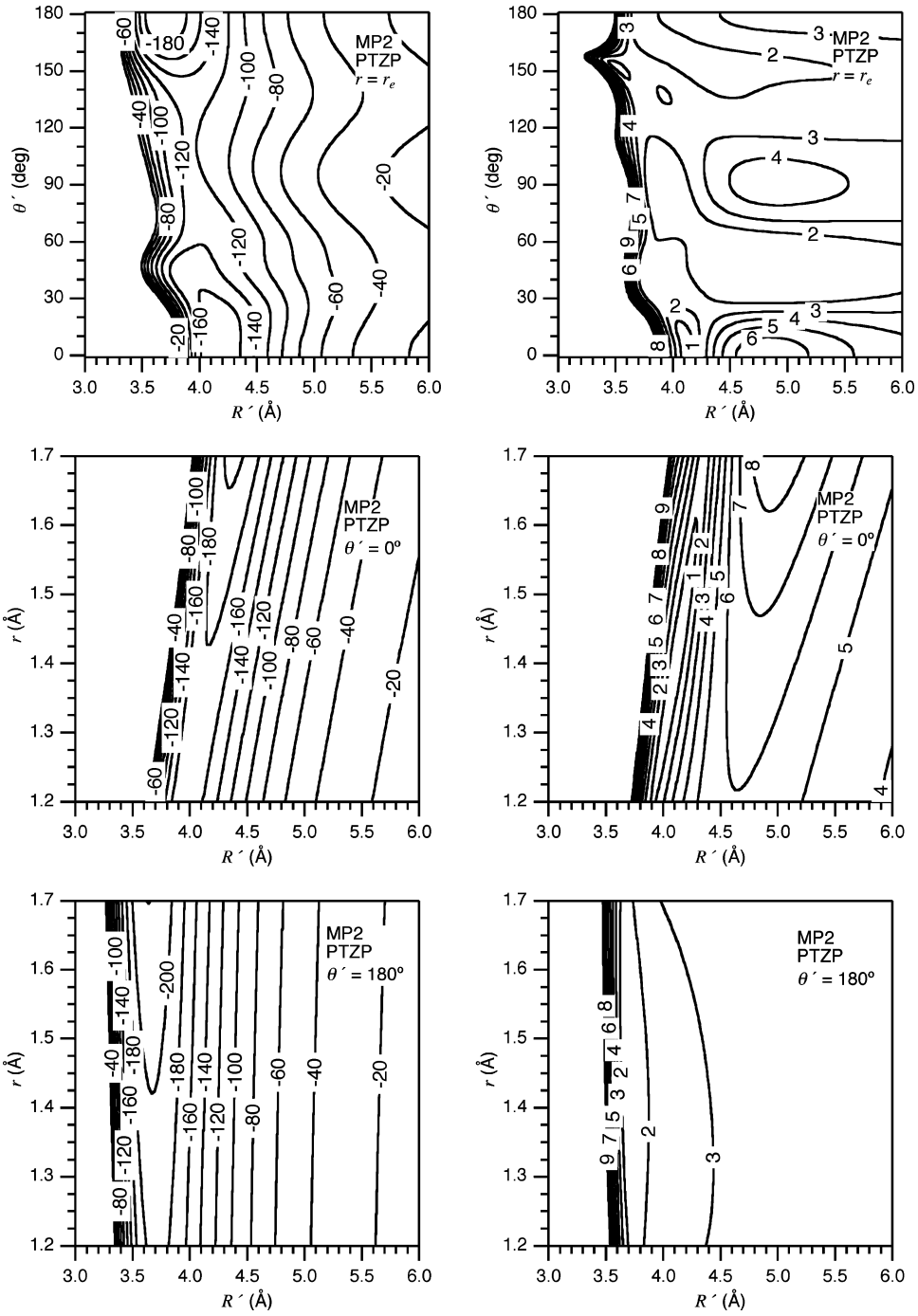

Figure 5. Morphed MP2P interaction potential of Ar−HBr. See the caption of Figure 3 for additional details.

correlation matrixes are given in Tables 6, 7, and 8, indicating that there is very little linear dependence among the final sets of morphing parameters leading to the relatively small uncertainties in the determined parameters.

As can be seen from this Table 5, somewhat fewer parameters were required for the potentials based on the correlation-consistent basis sets, and the CCSD(T) potential required fewer parameters than the MP2 potential. Thus, as might be expected, the CCSD(T) calculation gives a potential that is closer to the final morphed potential than do the potentials based on the MP2 calculations.[21]

Values of the morphed potentials and their corresponding statistical uncertainties are given in Figures 3, 4, and 5. The locations and energies of various stationary points are given in numerical form in Table 9 for both the morphed and unmorphed potentials. In Figure 6, the difference between the morphed CCCC potential and the morphed MP2P and MP2CC potentials are given. Results from the MP2CC and CCCC morphed potentials are seen to be somewhat in better agreement with each other than are the CCCC and MP2P potentials. In the regions around the minima, the MP2CC and CCCC potentials differ by less than 1 cm^{-1}, whereas the difference between the CCCC and MP2P potential at the global minimum is slightly more than 10 cm^{-1}.

Assuming that the CCCC morphed potential is our most accurate potential, we now estimate that the vdW minimum ($\theta = 180°$) is 11.9 ± 1.0 cm^{-1} lower in energy than the hydrogen-bond minimum ($\theta = 0°$). This value compares with previously determined values of[12] 20.9 and[11] 23.7(30) cm^{-1} and reflect the effect of scaling to the significantly larger value of D_0

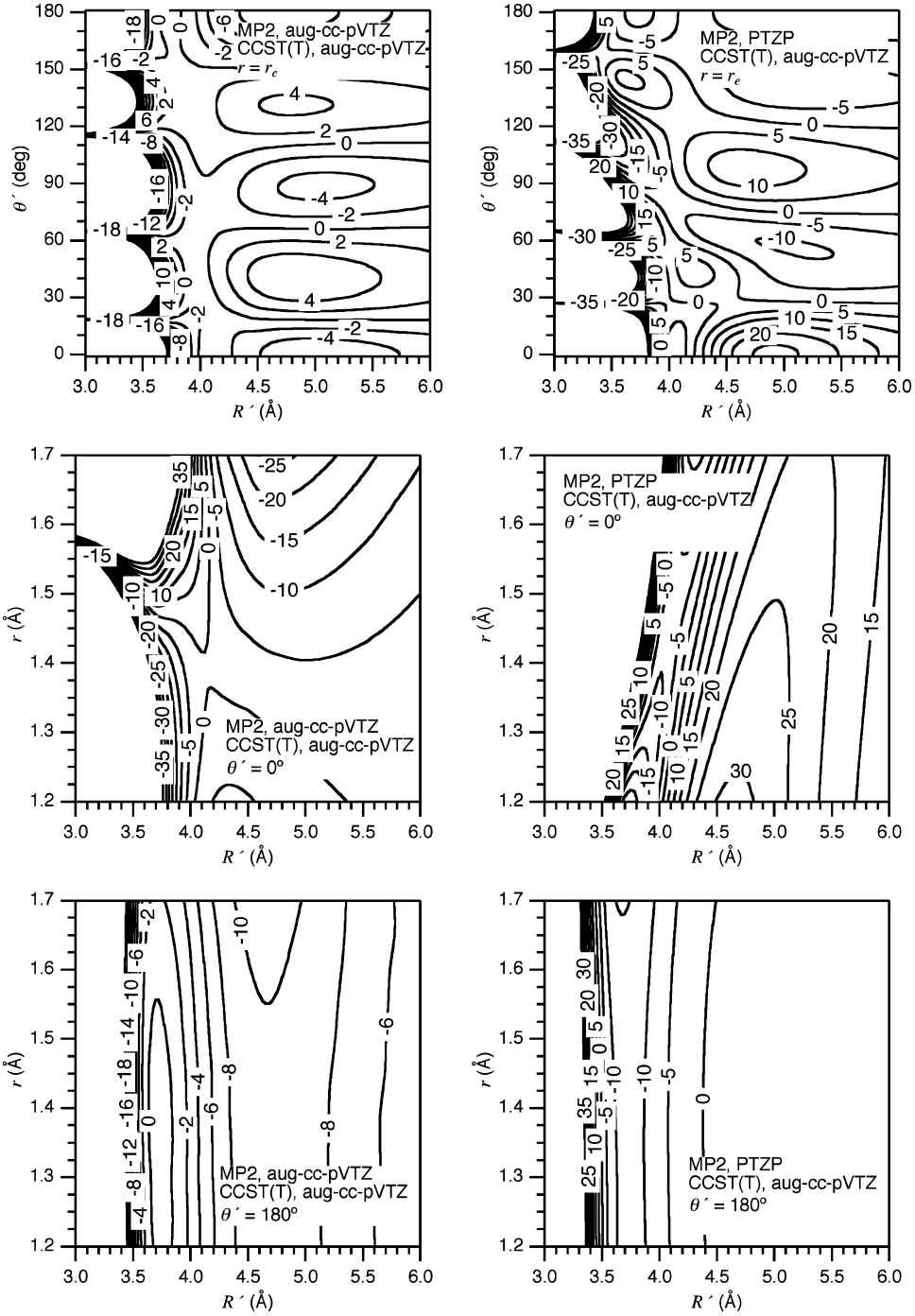

Figure 6. Differences between the morphed potentials. On the left-hand side is $V^{MP2CC} - V^{CCCC}$ and on the right-hand side is $V^{MP2P} - V^{CCCC}$. The three panels on each side are the three cuts through differences as described in Figure 3. See the caption of Figure 3 for additional details.

TABLE 9: Features of the Morphed and Unmorphed Potentials with $r = r_e$

	$\theta = 180°$ minimum		saddle point			$\theta = 0°$ minimum	
potential	V_{min}/cm^{-1}	$R_{min}/Å$	V_{saddle}/cm^{-1}	$R_{saddle}/Å$	$\theta_{saddle}/(deg)$	V_{min}/cm^{-1}	$R_{min}/Å$
MP2P unmorphed	−136.6	3.80	−79.9	4.18	108	−143.1	4.28
MP2CC unmorphed	−167.3	3.72	−100.0	4.10	100	−174.2	4.20
CCCC unmorphed	−131.5	3.80	−83.0	4.15	101	−144.4	4.26
MP2P morphed	−199.6	3.67	−121.0	3.91	112	−179.4	4.15
MP2CC morphed	−187.9	3.64	−118.5	3.99	106	−177.6	4.23
CCCC morphed	−188.3	3.67	−118.9	3.99	104	−176.4	4.20

determined from our experimental results. This investigation, however, confirms the previously made conclusion in which the ground state and the global minima are determined to have different isomeric structures. The value of D_0 for Ar−HBr of 130 cm^{-1} is consistent with the trend seen in the lighter members of the homologous series, Ar−HX, for which the values are 101.7(1.2) cm^{-1} in[28] Ar−HF and 114 cm^{-1} in[49] Ar−HCl. We note however that D_0 for the other isomer Ar−BrH

has a value of 118(1) cm^{-1}. Corresponding values of D_e are determined to be 176(1) and 188(1) cm^{-1} for Ar−HBr and Ar−BrH, respectively.

V. Conclusions

Rotational predissociative line broadening in υ_1 Ar−HBr has been experimentally investigated using IR diode laser spectroscopy, and D_0 was determined to be 130(1) cm^{-1} from the radial scattering equations. This result can be compared with predictions of 84.2, 117.9, and 94.7 cm^{-1} based on the MP2P, MP2CC, and CCCC calculations. The MP2CC calculation thus provides the most accurate prediction of D_0, only ∼10% lower than the experimentally determined value. Corresponding morphed global potential minima of 199.6, 187.9, and 188.3 cm^{-1} indicate that the morphed MP2P global minimum appears to overestimate the values based on MP2CC and CCCC morphed potentials in this case by approximately 10 cm^{-1}. This difference in final morphed potentials between MP2P and MP2CC is due to both the use of different one-electron basis sets and the use of different interpolation grids. Finally, the results of the current investigations give further confirmation that the ground state of Ar−HBr is the Ar−HBr isomer, but Ar−BrH is the corresponding global minimum that is 12 ± 1 cm^{-1} more stable than the Ar−HBr local minimum.

Acknowledgment. We are grateful to the National Science Foundation and the Center for Atmospheric Chemistry and the Environment, Texas A&M University for financial support for this research. J. W. Bevan expresses gratitude to the Robert A. Welch Foundation (Grant A-747) for financial support including predoctoral fellowships for A. L. McIntosh and B. A. McElmurry.

References and Notes

(1) Buchachenko, A. A.; Stepanov, N. F.; Krems, R. V.; Nordholm, S. *Phys. Chem. Chem. Phys.* **2002**, *4*, 4992.
(2) Nesbitt, D. J.; Child, M. S.; Clary, D. C. *J. Chem. Phys.* **1989**, *90*, 4855.
(3) Hutson, J. M. *J. Chem. Phys.* **1992**, *96*, 6752.
(4) Hutson, J. M. *J. Phys. Chem.* **1992**, *96*, 4237.
(5) Hutson, J. M. *J. Chem. Phys.* **1989**, *91*, 4455.
(6) Chang, H.-C.; Tao, F.-M.; Klemperer, W.; Healey, C.; Hutson, J. M. *J. Chem. Phys.* **1993**, *99*, 9337.
(7) Shroll, R. M.; Lohr, L. L.; Barker, J. R. *J. Chem. Phys.* **2001**, *115*, 4573.
(8) Woon, D. E.; Peterson, K. A.; Dunning, T. H., Jr. *J. Chem. Phys.* **1998**, *109*, 2233.
(9) Geremia, J. M.; Rabitz, H. *J. Chem. Phys.* **2001**, *115*, 8899.
(10) Clary, D. C. *Mol. Phys.* **2002**, *100*, 149.
(11) Belov, S. P.; McElmurry, B. A.; Lucchese, R. R.; Bevan, J. W.; Leonov, I. *Chem. Phys. Lett.* **2003**, *370*, 528.
(12) Castillo-Chará, J.; Lucchese, R. R.; Bevan, J. W. *J. Chem. Phys.* **2001**, *115*, 899.
(13) Suzuki, T.; Katayanagi, H.; Heaven, M. C. *J. Phys. Chem. A* **1997**, *101*, 6697.
(14) Slavicek, P.; Roeselova, M.; Jungwirth, P.; Schmidt, B. *J. Chem. Phys.* **2001**, *114*, 1539.
(15) Prosmiti, R.; Lopez-Lopez, S.; Garcia-Vela, A. *J. Chem. Phys.* **2004**, *120*, 6471.
(16) McIntosh, A.; Wang, Z.; Castillo-Chará, J.; Lucchese, R. R.; Bevan, J. W.; Suenram, R. D.; Legon, A. C. *J. Chem. Phys.* **1999**, *111*, 5764.
(17) McElmurry, B. A.; Lucchese, R. R.; Bevan, J. W.; Belov, S. P. *Phys. Chem. Chem. Phys.* **2004**, *6*, 5318.
(18) Prosmiti, R.; Garcia-Vela, A. *Chem. Phys. Lett.* **2002**, *366*, 238.
(19) Buck, U. *J. Phys. Chem. A* **2002**, *106*, 10049.
(20) Han, J.; McIntosh, A. L.; Wang, Z.; Lucchese, R. R.; Bevan, J. W. *Chem. Phys. Lett.* **1997**, *265*, 209.
(21) Meuwly, M.; Hutson, J. M. *J. Chem. Phys.* **1999**, *110*, 8338.
(22) Bevan, J. W.; Legon, A. C.; Rego, C. A.; Roach, J. *Chem. Phys. Lett.* **1992**, *198*, 347.
(23) Oudejans, L.; Nauta, K.; Miller, R. E. *J. Chem. Phys.* **1996**, *105*, 10410.
(24) Bevan, J. W.; Legon, A. C.; Rego, C. A. *Chem. Phys. Lett.* **1993**, *204*, 551.
(25) Tannenbaum, E.; Higgins, K. J.; Klemperer, W.; Segev, B.; Heller, E. J. *J. Phys. Chem. B* **2002**, *106*, 8100.
(26) Oudejans, L.; Miller, R. E. *Annu. Rev. Phys. Chem.* **2001**, *52*, 607.
(27) Harada, K.; Tanaka, K.; Tanaka, T.; Nanbu, S.; Aoyagi, M. *J. Chem. Phys.* **2002**, *117*, 7041.
(28) Fraser, G. T.; Pine, A. S. *J. Chem. Phys.* **1986**, *85*, 2502.
(29) Wang, Z.; McIntosh, A. L.; Lucchese, R. R.; Bevan, J. W. *J. Mol. Struct.* **2004**, *695*−*696*, 171.
(30) Guelachvili, G.; Rao, K. N. *Handbook of Infrared Standards*; Academic Press: New York, 1986.
(31) Busarow, K. L.; Blake, G. A.; Laughlin, K. B.; Cohen, R. C.; Lee, Y. T.; Saykally, R. J. *Chem. Phys.* Lett. **1987**, *141*, 289.
(32) Demtröder, W. *Laser spectroscopy: Basic concepts and instrumentation*, 2nd ed.; Springer: Berlin, Germany, 1996.
(33) *Mathematica*, 5.1 ed.; Wolfram Research: Urbana, Illinois, 2005.
(34) Frisch, M. J.; Trucks, G. W.; Schlegel, H. B.; Scuseria, G. E.; Robb, M. A.; Cheeseman, J. R.; Montgomery, J. A., Jr.; Vreven, T.; Kudin, K. N.; Burant, J. C.; Millam, J. M.; Iyengar, S. S.; Tomasi, J.; Barone, V.; Mennucci, B.; Cossi, M.; Scalmani, G.; Rega, N.; Petersson, G. A.; Nakatsuji, H.; Hada, M.; Ehara, M.; Toyota, K.; Fukuda, R.; Hasegawa, J.; Ishida, M.; Nakajima, T.; Honda, Y.; Kitao, O.; Nakai, H.; Klene, M.; Li, X.; Knox, J. E.; Hratchian, H. P.; Cross, J. B.; Bakken, V.; Adamo, C.; Jaramillo, J.; Gomperts, R.; Stratmann, R. E.; Yazyev, O.; Austin, A. J.; Cammi, R.; Pomelli, C.; Ochterski, J. W.; Ayala, P. Y.; Morokuma, K.; Voth, G. A.; Salvador, P.; Dannenberg, J. J.; Zakrzewski, V. G.; Dapprich, S.; Daniels, A. D.; Strain, M. C.; Farkas, O.; Malick, D. K.; Rabuck, A. D.; Raghavachari, K.; Foresman, J. B.; Ortiz, J. V.; Cui, Q.; Baboul, A. G.; Clifford, S.; Cioslowski, J.; Stefanov, B. B.; Liu, G.; Liashenko, A.; Piskorz, P.; Komaromi, I.; Martin, R. L.; Fox, D. J.; Keith, T.; Al-Laham, M. A.; Peng, C. Y.; Nanayakkara, A.; Challacombe, M.; Gill, P. M. W.; Johnson, B.; Chen, W.; Wong, M. W.; Gonzalez, C.; Pople, J. A. *Gaussian 03*, revision C.02; Gaussian, Inc.: Wallingford, CT, 2004.
(35) Dunning, T. H., Jr. *J. Chem. Phys.* **1989**, *90*, 1007.
(36) Woon, D. E.; Dunning, T. H., Jr. *J. Chem. Phys.* **1993**, *98*, 1358.
(37) Wilson, A. K.; Woon, D. E.; Peterson, K. A.; Dunning, T. H. J. *J. Chem. Phys.* **1999**, *110*, 7667.
(38) Werner, H.-J.; Knowles, P. J.; Lindh, R.; Schutz, M.; Celani, P.; Korona, T.; Manby, F. R.; Rauhut, G.; Amos, R. D.; Bernhardsson, A.; Berning, A.; Cooper, D. L.; Deegan, M. J. O.; Dobbyn, A. J.; Eckert, F.; Hampel, C.; Hetzer, G.; Lloyd, A. W.; McNicholas, S. J.; Meyer, W.; Mura, M. E.; Nicklass, A.; Palmieri, P.; Pitzer, R.; Schumann, U.; Stoll, H.; Stone, A. J.; Tarroni, R.; Thorsteinsson, T. *MOLPRO, a package of ab initio programs*, 2002.6 ed.; Birmingham, U.K., 2003.
(39) Huber, K. P.; Herzberg, G. *Molecular Spectra and Molecular Structure IV. Constants of Diatomic* Molecules; Van Nostrand Reinhold Co.: New York, 1979.
(40) Boys, S. F.; Bernardi, F. *Mol. Phys.* **1970**, *19*, 553.
(41) Hulburt, H. M.; Hirschfelder, J. O. *J. Chem. Phys.* **1941**, *9*, 61.
(42) Rank, D. H.; Fink, U.; Wiggins, T. A. *J. Mol. Spectrosc.* **1965**, *18*, 170.
(43) Ho, T.-S.; Rabitz, H. *J. Chem. Phys.* **1996**, *104*, 2584.
(44) Lin, P.; Jabs, W.; Lucchese, R. R.; Bevan, J. W.; Brugh, D. J.; Suenram, R. D. *Chem. Phys. Lett.* **2002**, *356*, 101.
(45) Soldan, P.; Hutson, J. M. *J. Chem. Phys.* **2000**, *112*, 4415.
(46) McIntosh, A.; Gallegos, A. M.; Lucchese, R. R.; Bevan, J. W. *J. Chem. Phys.* **1997**, *107*, 8327.
(47) Quinones, A.; Bandarage, G.; Bevan, J. W.; Lucchese, R. R. *J. Chem. Phys.* **1992**, *97*, 2209.
(48) Press, W. H.; Flannery, B. P.; Teukolsky, S. A.; Vetterling, W. T. *Numerical Recipes. The Art of Scientific Computing*; Cambridge University Press: Cambridge, U.K., 1986.
(49) Howard, B. J.; Pine, A. S. *Chem. Phys. Lett.* **1985**, *122*, 1.
(50) Firth, D. W.; Dvorak, M. A.; Reeve, S. W.; Ford, R. S.; Leopold, K. R. *Chem. Phys. Lett.* **1990**, *168*, 161.
(51) Jackson, K. C.; Langridge-Smith, P. R. R.; Howard, B. J. *Mol. Phys.* **1980**, *39*, 817.
(52) Keenan, M. R.; Campbell, E. J.; Balle, T. J.; Buxton, L. W.; Minton, T. K.; Soper, P. D.; Flygare, W. H. *J. Chem. Phys.* **1980**, *72*, 3070.